



Jet Noise Reduction by Microjets—A Parametric Study

K.B.M.Q. Zaman
Glenn Research Center, Cleveland, Ohio

NASA STI Program . . . in Profile

Since its founding, NASA has been dedicated to the advancement of aeronautics and space science. The NASA Scientific and Technical Information (STI) program plays a key part in helping NASA maintain this important role.

The NASA STI Program operates under the auspices of the Agency Chief Information Officer. It collects, organizes, provides for archiving, and disseminates NASA's STI. The NASA STI program provides access to the NASA Aeronautics and Space Database and its public interface, the NASA Technical Reports Server, thus providing one of the largest collections of aeronautical and space science STI in the world. Results are published in both non-NASA channels and by NASA in the NASA STI Report Series, which includes the following report types:

- **TECHNICAL PUBLICATION.** Reports of completed research or a major significant phase of research that present the results of NASA programs and include extensive data or theoretical analysis. Includes compilations of significant scientific and technical data and information deemed to be of continuing reference value. NASA counterpart of peer-reviewed formal professional papers but has less stringent limitations on manuscript length and extent of graphic presentations.
- **TECHNICAL MEMORANDUM.** Scientific and technical findings that are preliminary or of specialized interest, e.g., quick release reports, working papers, and bibliographies that contain minimal annotation. Does not contain extensive analysis.
- **CONTRACTOR REPORT.** Scientific and technical findings by NASA-sponsored contractors and grantees.

- **CONFERENCE PUBLICATION.** Collected papers from scientific and technical conferences, symposia, seminars, or other meetings sponsored or cosponsored by NASA.
- **SPECIAL PUBLICATION.** Scientific, technical, or historical information from NASA programs, projects, and missions, often concerned with subjects having substantial public interest.
- **TECHNICAL TRANSLATION.** English-language translations of foreign scientific and technical material pertinent to NASA's mission.

Specialized services also include creating custom thesauri, building customized databases, organizing and publishing research results.

For more information about the NASA STI program, see the following:

- Access the NASA STI program home page at <http://www.sti.nasa.gov>
- E-mail your question via the Internet to help@sti.nasa.gov
- Fax your question to the NASA STI Help Desk at 443-757-5803
- Telephone the NASA STI Help Desk at 443-757-5802
- Write to:
NASA Center for AeroSpace Information (CASI)
7115 Standard Drive
Hanover, MD 21076-1320



Jet Noise Reduction by Microjets—A Parametric Study

K.B.M.Q. Zaman
Glenn Research Center, Cleveland, Ohio

Prepared for the
15th AIAA/CEAS Aeroacoustics Conference (30th AIAA Aeroacoustics Conference)
cosponsored by AIAA and CEAS
Miami, Florida, May 11–13, 2009

National Aeronautics and
Space Administration

Glenn Research Center
Cleveland, Ohio 44135

Acknowledgments

The author would like to thank Professor Anjaneyulu Krothapalli of Florida State University and colleagues, John Abbott and Nicholas Georgiadis for helpful comments. Support from the Subsonic Fixed Wing Project and the Supersonics Project, under NASA Fundamental Aeronautics Program, is gratefully acknowledged.

This report contains preliminary findings,
subject to revision as analysis proceeds.

Trade names and trademarks are used in this report for identification
only. Their usage does not constitute an official endorsement,
either expressed or implied, by the National Aeronautics and
Space Administration.

This work was sponsored by the Fundamental Aeronautics Program
at the NASA Glenn Research Center.

Level of Review: This material has been technically reviewed by technical management.

Available from

NASA Center for Aerospace Information
7115 Standard Drive
Hanover, MD 21076-1320

National Technical Information Service
5285 Port Royal Road
Springfield, VA 22161

Available electronically at <http://gltrs.grc.nasa.gov>

Jet Noise Reduction by Microjets—A Parametric Study

K.B.M.Q. Zaman
National Aeronautics and Space Administration
Glenn Research Center
Cleveland, Ohio 44135

Abstract

The effect of injecting tiny secondary jets (' μ jets') on the radiated noise from a subsonic primary jet is studied experimentally. The μ jets are injected on to the primary jet near the nozzle exit with variable port geometry, working fluid and driving pressure. A clear noise reduction is observed that improves with increasing μ jet pressure. It is found that smaller diameter ports with higher driving pressure, but involving less thrust and mass fraction, can produce better noise reduction. A collection of data from the present as well as past experiments is examined in an attempt to correlate the noise reduction with the operating parameters. The results indicate that turbulent mixing noise reduction, as monitored by OASPL at a shallow angle, correlates with the ratio of μ jet to primary jet driving pressures normalized by the ratio of corresponding diameters ($p_{\mu}d/p_jD$). With gaseous injection, the spectral amplitudes decrease at lower frequencies while an increase is noted at higher frequencies. It is apparent that this amplitude 'crossover' is at least partly due to shock-associated noise from the underexpanded μ jets themselves. Such crossover is not seen with water injection since the flow in that case is incompressible and there is no shock-associated noise. Centerline velocity data show that larger noise reduction is accompanied by faster jet decay as well as significant reduction in turbulence intensities. While a physical understanding of the dependence of noise reduction on $p_{\mu}d/p_jD$ remains unclear, given this correlation, an analysis explains the observed dependence of the effect on various other parameters.

Nomenclature

d	microjet (μ jet) port exit diameter
D	primary nozzle exit diameter
I	overall sound pressure level (OASPL)
J	momentum flux ratio = $\rho_{\mu}U_{\mu}^2/\rho_jU_j^2$
k	specific heat ratio
m	mass fraction = mass flow rate of all μ jets / mass flow rate of primary jet
M	Mach number
M_J	$= \left(\left(\left(p_j/p_a \right)^{(k-1)/k} - 1 \right) \frac{2}{k-1} \right)^{1/2}$ ("Fully expanded jet Mach number")
M_{ej}	Mach number at exit of primary nozzle
n	number of equally spaced μ jets
p	supply (total) pressure for primary jet or μ jet
r_m	mass fraction per μ jet = m/n
SPL	sound pressure level
t	T_{μ}/T_j (ratio of total thrust of all μ jets to thrust of primary jet)
U	mean velocity at exit of jet nozzle or μ jet port
ρ	density at exit of jet nozzle or μ jet port
θ	microphone angular (polar) location, relative to downstream jet axis
ϕ	μ jet injection yaw angle relative to radial direction
φ	μ jet injection pitch angle relative to primary nozzle exit plane

Subscripts

a	ambient
j	primary jet
μ	μ jet

1.0 Introduction

Stricter regulations on aircraft noise have prompted numerous efforts addressing jet noise reduction. One technique receiving renewed attention is the use of ‘microjets’ (referred to as ‘ μ jets’). It evolved from past studies on noise reduction with water as well as gaseous injection and simply involves impingement of tiny secondary jets on to the primary jet near the nozzle lip (Refs. 1 to 13). The concept dates back to the 1950s (e.g., Refs. 12 and 13) provides a literature review covering the five decades since. While a detailed review of past work is not central to this paper, a few pertinent points are important to note.

First, water injection, used routinely in noise suppression for rocket nozzles during launch, requires a large mass fraction (water to jet exhaust mass ratio in the order of unity) (Ref. 11). This is obviously not feasible in aircraft flight where the mass fraction must be kept to an absolute minimum. There is growing evidence that noise benefit with small mass fraction may be possible with higher injection pressures (Refs. 6 and 13). Pushing this aspect of the technique to its limits, within the facility constraints, is an objective of the present study.

Second, as with some other noise reduction techniques, μ jets have been shown to produce large effects on supersonic primary jets. This is apparently due to a weakening of shock structure resulting in an attenuation of shock-associated noise. Reference 3 reports up to 6 dB noise reduction, with mitigation of all of Mach wave radiation. A reduction of turbulent mixing noise, as occurring in a high subsonic jet, however, is far more challenging and holds the key to noise abatement in many aircraft. With the μ jets, a moderate but consistent noise reduction has been observed in high subsonic jets (Refs. 6, 9, 10, and 14). The scope of the present investigation is limited to the latter flow regime for an unambiguous study of the effect on turbulent mixing noise.

Furthermore, very little has been known about the dependence of the noise attenuation by the μ jets on the operating parameters. Reference 3 noted a correlation with the momentum flux ratio (J), however, the data were limited. The study pertained to supersonic jets, leaving it unclear how the mixing noise and the shock-associated noise components were individually affected. Results in Reference 14 suggested that J might not be the best parameter to correlate mixing noise attenuation. In this study, an attempt is made to find such correlations and underlying trends in turbulent mixing noise attenuation by the μ jets, by scrutinizing a collection of experimental data.

The present study was initiated a few years ago in an effort to explore the full potential of the μ jet effect and advance the understanding of its mechanisms. First, the effect of air μ jets was explored with variable port geometry and driving pressure while paying attention to estimated thrust and mass fraction requirements. The results were summarized in Reference 14. A key observation was that the reduction in OASPL in the direction of peak noise radiation scaled with the ratio of the density-velocity-diameter product of the μ jet to that of the primary jet. In following experiments, gaseous CO₂ and liquid H₂O were also used as working fluid. The limit of μ jet driving pressure was pushed to twice the value covered earlier. The new results confirmed the scaling law noted in Reference 14 but only for gaseous injection. With water injection, large deviation from the correlation occurred. A normalized pressure parameter was then found to correlate all the data. Even though a complete physical understanding of this correlation remains from being clear, the experimental findings are deemed significant enough to merit documentation. The objective of this paper is to describe these results and provide an analysis and discussion.

2.0 Experimental Facility

The experiments were conducted in an open jet facility at the NASA Glenn Research Center (Fig. 1(a)). The primary jet issued from a convergent nozzle with exit diameter, $D = 37.6$ mm. The μ jets were injected via a ring manifold mounted on the primary nozzle (Fig. 1(b)). The surfaces were machined such that when placed all the way in the manifold sat flush with the lip of the nozzle. It was supplied with compressed air from a pressurized source ('K-bottle'). There were six threaded outlets which could be fitted with tiny screws (similar in size as used with eyeglasses). The μ jets issued from ports and passages machined in these screws. Different sets of screws provided different port geometries. A picture of the manifold, with one of the screws in the foreground, is shown in Figure 1(c).

Dimensions of the manifold and the ports are shown schematically in Figure 2(a). Data from cylindrical ports with diameters, $d = 0.203$ and 0.102 mm will be presented in this paper. The ports were drilled in the brass screws with a tolerance of ± 0.005 mm. For a given set, the number of ports could be varied by blanking off some of the outlets with 'blind' screws. Each screw could also be turned to inject the μ jet at a desired yaw angle (ϕ) relative to the radial direction (Fig. 2(b)). The injection pitch angle (ψ) was zero in the present experiment. Note that there is a total stand-off distance of 0.89 mm in the radial direction between the port exit and the periphery of the jet, 0.76 mm being the thickness of the nozzle lip. The manifold could also be positioned with a stand-off distance, Δx , in the axial direction with respect to the nozzle lip.

For the smaller ports in the present experiment the diameter ratio d/D is 0.0027 which is smaller than that in previous studies. For example, the smallest d/D was 0.0038 , 0.012 , 0.018 , and 0.020 in References 5, 4, 6, and 10, respectively. Based on the diameter ratio, the attribute 'microjet' is obviously a misnomer but it has prevailed in the literature. Also, much higher injection pressures, up to 12.3 mPa (1770 psig), were investigated in the present study compared to, for example, 5.6 mPa in References 3 and 14. Note that the spectral data acquisition took about 35 sec during which the bottle pressure would drop by several hundred kPa depending on regulator pressure and port size. Thus, the choice of maximum working pressure was somewhat lower even though bottle pressure up to 14.5 mPa was available, in order to ensure a constant pressure during runs. It should also be noted that the data presented in this paper were obtained in many sessions over a period of several months. The chosen pressure (p_μ) for various sets of data was sometimes dictated by available bottle pressure. Thus, the reader may notice some inconsistencies in the choice of p_μ from figure to figure but this did not impact the conclusions.

The CO_2 injection was done with the same hardware covering pressures up to about 5.5 mPa (limited by liquefaction at room temperature). For water injection, a 1.9 cm i.d., U-shaped, stainless steel tube was placed in the supply line (Fig. 1(a)). The 4 m long tube was filled with distilled water making sure there were no air pockets. The column of water was driven by compressed air and the rest of the hardware was unchanged. Unfortunately, clogging occurred with water injection possibly due to some sort of residues depositing within the tiny ports. The problem aggravated with the smaller 0.1 mm ports and impacted data repeatability as discussed later. Water injection data from the 0.2 mm ports only are to be presented.

The exit flow properties of the μ jets including the mass fraction were calculated from the supply pressure p_μ and the port diameter, using isentropic nozzle flow equations. The pressure was measured at the regulator just downstream of the K-bottle. With the larger ports there was a pressure drop in the supply line, as determined by separate measurements, by about 10 percent. All pressures (p_μ) were corrected to represent the pressure within the manifold. Some of the data from the literature, to be compared with in the following, involved direct measurement of the mass fraction m . The pressure p_μ and other exit properties for these cases were calculated from the m data using the nozzle flow equations. Note that in all calculations boundary layer effects were neglected, i.e., the discharge coefficient was assumed unity.

The far-field noise was measured with (B&K model 4135) microphones located at 37 and $50 D$ from the nozzle exit for $\theta = 90^\circ$ and 25° , respectively. The microphone angular location θ is referenced with respect to the downstream jet axis in this paper (Fig. 2(b)). Most of the data presented are for $\theta = 25^\circ$, the

direction of peak noise radiation. The spectral data reported earlier in Reference 14 were obtained with a Nicolet 660B analyzer. Later, the data acquisition was done by a PC based system together with National Instruments hardware and Labview software. Spectral analysis was done digitally and the OASPL data were obtained by integration of the spectra. Figure 1(a) indicates that the test environment was less than ideal for noise measurement. However, a comparison with data from other facilities showed that the spectral amplitudes were within a facility-to-facility scatter band of about 2 dB (Ref. 15). The data quality is considered adequate for studying the effect of the μ jets relative to the baseline (no- μ jet) case. Note, however, that the differences in the OASPL values in some cases bordered on the limits of data repeatability. The test chamber was climate-controlled and care was taken to ensure best possible measurement conditions. The data for the baseline as well as a few other cases were repeated several times over a period of several months. The scatter in the OASPL values is discussed shortly in the following sections.

Standard Pitot probe and single hot-wire techniques were used to measure centerline variation of flow properties. Caveats in these measurements will be discussed together with the results. Flow visualization pictures were obtained for the water injection case. All data acquisition, activation of the μ jet and setting its pressure as well as flow visualization were done under remote computer control. All results presented in this paper are for cold flow, i.e., with the total temperature the same everywhere as in the ambient.

3.0 Results

For the earlier results reported in Reference 14, the μ jet parameters were varied within the constraints of the experimental facility, while looking for maximum noise reduction. Noise spectra were compared while varying injector yaw, arrangement, number, geometry, etc. Key results are narrated here and an interested reader may find details in the cited paper. It was found that yawing the μ jets improved noise reduction relative to the case of radial injection; this is discussed further with Figure 3. In one arrangement, the yaw angle was alternated (positive and negative) for successive ports. The noise reduction with this geometry was smaller compared to that produced by six ports yawed in the same direction. Reducing the number of ports from six to three approximately halved the OASPL reduction at $\theta = 25^\circ$. Reference 10 reported optimum noise reduction with 18 ports when the number of ports was varied from 3 to 36. In fact, their OASPL reduction data (in dB) exhibited almost a linear variation with n , up to 18. This trend will be invoked when comparing the present results with data from the literature.

Figure 3 shows an important result from Reference 14. OASPL reduction is plotted as a function of the yaw angle. The circular symbols are for the 0.2 mm ports with $p_\mu = 3410$ kPa. For each data point, all six ports are yawed by the same angle (ϕ). The optimum reduction has occurred at $\phi = 45^\circ$. The three diamond symbols are for the 0.1 mm ports with $p_\mu = 6930$ kPa. The calculated mass fraction and thrust of the μ jets as well as momentum flux ratio for the two port cases are listed in Table 1. First, it is observed that for both ports a small additional reduction has been achieved with yaw relative to the zero-yaw case. For the smaller ports the optimum has occurred at $\phi = 25^\circ$ as compared to 45° with the larger ports. This shift is likely to be due to the stand-off distance between the port exit and the periphery of the jet (Fig. 2(a)). At 45° yaw, with the smaller port, the μ jet has to travel a longer relative distance (about $18d$, including the estimated shear layer thickness) before impinging on the core of the jet. Thus, the impact is diminished because of turbulent diffusion of the μ jet. This also explains the rapid drop-off of the effect for $\phi > 45^\circ$ with either port cases. It is evident that the noise reduction has improved with the smaller ports. By inspecting the properties listed in Table 1, the following trend is noted: smaller ports with higher pressure, involving less μ jet mass fraction and thrust, can produce better noise reduction. Thus, for radial injection ($\phi = 0^\circ$) an additional 0.4 dB reduction has been achieved with the smaller ports. This is achieved with 50 percent less mass fraction and thrust. This trend is confirmed with further data in the following.

Except for Figure 3, all data presented in this paper were obtained subsequent to the experiments of Reference 14. All results from the literature, to be discussed in the following, pertained to zero yaw.

Thus, for direct comparison the subsequent experiments were also done for zero yaw, foregoing the additional gain noted for $\phi \approx 45^\circ$. Figure 4 shows the effect of injection location, Δx (Fig. 2(a)). OASPL data for $\theta = 25^\circ$ are shown with and without injection from six 0.2 mm ports at $p_\mu = 4175$ kPa. For no-injection, the level has not changed with varying Δx except for some scatter and an average line is drawn through the data. With injection (diamond symbols) the levels are lower. Difference from the average line for the no-injection case denotes OASPL reduction. For $\Delta x = 0$ (manifold face flush with nozzle lip), a reduction by approximately 1.5 dB has been achieved. However, with even a slight increase in Δx , the reduction drops significantly. Norum (Ref. 4) also noted an increased noise reduction when the injection was done closer to the nozzle; however, his experiment addressed effect on shock-associated noise and involved large steps in the axial location of the injectors (in fractions of D rather than d). In Figure 4 the reduction is seen to level off for $\Delta x > 1$ mm. For larger Δx , the primary jet adjusts to the cylindrical passage of the manifold that effectively becomes the nozzle for the ensuing jet of slightly larger diameter. Since the μ jets are injected just downstream of the manifold face the relative injection location for this larger jet remains unchanged. This apparently explains the leveling off of the amplitude.

It should be mentioned here that the data of Figure 4 were actually obtained at the very end of the investigation but are shown first to also provide the reader with an idea about the scatter involved (the issue is further discussed at the end of Section 3.1). Data taken over several days are shown in Figure 4 exhibiting a scatter band of about 0.4 dB. However, the sets of OASPL reduction results to be presented in the following were obtained in single runs each and are thought to involve much less scatter, within 0.2 dB. Note that all subsequent results are for $\Delta x = 0$.

3.1 Noise Attenuation at $\theta = 25^\circ$ and Correlation With Operating Parameters

The most significant result of the investigation is introduced in Figure 5 and it calls for a step by step discussion. The OASPL reduction at $\theta = 25^\circ$ is shown as a function of mass fraction per injector in percent. First, let us focus on the data points bunched on a line on the left (diamond, right- and left-triangle symbols). These are for six 0.1 mm ports, the diamond symbol being for CO_2 injection and the other two for air. The diamond and right-triangles are for injection at a fixed $M_J (= 0.95)$ with variable p_μ while the left-triangles are for a fixed $p_\mu (= 7000$ kPa) and variable M_J . These data are congruent and the observed OASPL reduction is simply a function of the mass fraction for the given port diameter. Next to these on the right is another set of data for six 0.2 mm ports (circle, gradient and delta symbols). Here, the circles (CO_2) and the gradients (air) are for injection with variable p_μ at $M_J = 0.95$, while the deltas (air) are for variable M_J with $p_\mu = 5130$ kPa. As with the 0.1 mm ports, the data are also congruent. In spite of two working fluids the noise attenuation is dependent only on the injection mass fraction, for a given port diameter. By drawing a vertical line through these two sets of data it is also evident that more noise reduction is achieved with the smaller ports for a given mass fraction, corroborating the result discussed with Figure 3.

Also shown in Figure 5 are a few sets of data from the literature. Let us first consider the air injection cases. The data from Reference 10 (denoted ‘CSJB’) were approximately read off from their Figure 13. Reference 6 (denoted ‘AKSL’) quoted about 2 dB decrease in OASPL at $\theta = 30^\circ$. These data are shown and identified in the legend. Note that both experiments are for cold flows and air-in-air injection in high subsonic jets, as in the present case. Table 2 compares the operating parameters. In both References 6 and 10, 18 μ jets were used as opposed to 6 in the present experiment. In order to make a proper comparison, first one needs to consider the amplitudes. The collection of data involves different number of μ jets, observation angle, primary jet Mach number as well as pitch angle ($\varphi = 0^\circ$ in the present case versus 45° in the others). Unfortunately, the available database is not enough to understand and fully account for the differences in the effects of these parameters. It appears that by far the largest effect is due to the difference in the number (n) of μ jets. As stated in the foregoing, Reference 10 reported almost a linear variation of OASPL reduction with n , up to 18. The OASPL values, for six versus three ports, reported in Reference 14 also followed this trend. Thus, if 6 μ jets were used instead of 18 in the two cited experiments, one might expect the reductions to be approximately 3

times smaller. This rule has been followed in presenting those data in Figure 5. Additional effects due to differences in pitch (ϕ), jet Mach number (M_j) and polar location (θ) are ignored. While the latter parameters may affect the amplitudes somewhat, it should become evident shortly that the ‘collapse’ of the data hinges largely on the choice of the abscissa and exact scaling of the amplitudes may not be critical in the exercise that we embark on in the following.

Upon an inspection it should be evident that all three curves from ‘CSJB’ exhibit a peak followed by a dip and then again an increase with increasing r_m . (An interested reader may look up either Reference 10 or 14 to see these trends clearly with an amplified vertical scale.) The authors reasoned that the dip occurred when the μ jet transitioned from subsonic to supersonic regime. Specifically, the dips occurred just past the condition where the μ jets became supersonic when additional shock associated noise from themselves caused a drop in the measured noise reduction. However, with further increase in r_m eventually the trend of increasing noise reduction resumed. The present data do not exhibit such peaks and dips. This is simply because the μ jets are supersonic for the entire parametric range covered.

The solid symbols in Figure 5 are for water injection. The gradient data points are taken from Reference 4 that reports a detailed study covering subsonic and supersonic primary jets including high temperature effect. Two types of injection (spray versus jet) were explored while varying the number of injectors. Here, data for a condition close to the present case are compared—six injectors for a cold primary jet at $M_j = 0.8$ (case ‘J2/06/45’). The raw directivity data ($30^\circ < \theta < 135^\circ$), kindly provided by the author, showed noise reduction at most angular locations with some scatter. Data for $\theta = 32.5^\circ$ are shown. As stated in Section 2, while the mass fraction for the present experiment was estimated from the driving pressure, it was measured directly in Reference 4 as well as Reference 10. On the other hand, while p_μ was measured directly in the present experiment it was deduced from the mass fraction data for the cited cases. The solid triangular symbols in Figure 5 represent water injection result from the present experiment. These fall to the left of the data of Reference 4. Since Reference 4 involves much larger ports (1.6 mm), it can be inferred that water injection with the smaller (0.2 mm) ports has also yielded better noise reduction at a given r_m , in a similar manner as seen with the gaseous injection cases. It is also noted that the data for water and gaseous injection from the present experiment, with the same set of (0.2 mm) ports, are separated by an order of magnitude in the abscissa. Clearly the noise reduction does not depend on the parameter r_m alone. Neither would the data ‘collapse’ if plotted as a function of the total mass fraction ($m = r_m \times n$). For example, the present air-injection data falling to the left of the data from References 6 and 10 would move further to the left since only 6 ports are used as opposed to 18 in the latter cases.

An attempt is made to explore if a certain combination of parameters would collapse the data of Figure 5, with the expectation that such an exercise might provide insight into the scaling as well as the underlying mechanism. The data are plotted and compared with various parameters for the abscissa. In order to make a ‘fair’ comparison the abscissa scales in all plots are chosen to span 4 decades. Figure 6 shows the result as a function of the ratio of density-velocity-diameter product. It is apparent that all the gaseous injection data have collapsed reasonably. This was a key observation in Reference 14 that is confirmed with a larger variation in p_μ and an additional working fluid for the μ jet. It is also immediately clear that the water injection data have not followed the correlation. In Figure 7, the data are plotted as a function of the thrust fraction. Here, T_μ represents calculated total thrust of the μ jets. Clearly, the data are far from collapsed. Similarly, a lack of collapse is noted when the data are plotted as a function of the momentum flux ratio J (Fig. 8); the effect of J will be further discussed in Sections 3.4 and 3.5. Similar exercise with velocity ratio, U_μ/U_j , velocity-density product ratio, $\rho_\mu U_\mu/\rho_j U_j$, or the quantity r_m/d^2 (as explored in Reference 10) failed to produce a reasonable collapse.

The best collapse occurred when the data were plotted as a function of the ratio of the driving pressures normalized by the ratio of the diameters, as shown in Figure 9. Practically all data now fall in a continuous band. Thus, the noise reduction appears to correlate with the parameter $p_\mu d/p_j D$. Note that the database for reaching this correlation pertains to high subsonic jets and in the direction of peak noise radiation. Thus, the correlation applies to turbulent mixing noise reduction.

As stated before, for comparing the relative collapse, the data in Figure 9 are shown with the abscissa spanning four decades. Thus, the curves are squeezed together and might hide finer trends. In Figure 10, the same data are examined with an expanded linear abscissa. There are conspicuous differences among the different sets; however, no clear trend is apparent. The water injection data from the present experiment exhibit the largest deviation. The lower amplitudes for this case are thought to be partly due to the clogging of the ports as discussed in Section 2. Some of the data points within this set are repeats from later runs and exhibit the largest scatter. Ignoring this set, the rest of the data fall within a cluster that could be represented by a linear correlation,

$$\Delta I = 12.0 p_{\mu} d / p_j D \quad (1)$$

where ΔI is OASPL reduction at a shallow angle. Note again that $p_{\mu} d / p_j D$ applies to the condition for each μ jet and ΔI represents noise reduction achieved by using six μ jets.

With regards to the repeatability of the data, referring back to the discussion of Figure 4, it should be noted that after the water injection experiment discrepancies occurred even with air injection when trying to repeat some measurements. Although the injectors were cleansed in ultrasonic baths, the amplitudes especially with the 0.1 mm ports were lower. The larger ports could be restored mechanically by inserting a drill bit under microscope but this was not possible with the more fragile drill bit for the smaller ports. A new set of injectors was fabricated but it turned out that the stand-off distance of the ports was different, ($\delta \approx 0.25$ instead of 0.13 mm; Fig. 2), and the results could not be reproduced. However, the basic trends in the relative amplitudes remained valid. These deliberations prompted the experiment described with Figure 4. Subsequent flow-field experiments described in Section 3.3 were conducted only with the 0.2 mm ports.

3.2 Noise Attenuation at $\theta = 90^\circ$ and Self Noise From μ jets

In previous investigations, the noise reduction by the μ jets was noted at shallow as well as large angles. This is seen from the directivity plots of References 4 and 5 for high subsonic jets and Reference 3 for imperfectly expanded supersonic jets. In the present experiment data were acquired only at 25° and 90° . While the 25° data, discussed so far, exhibit consistent noise reduction the results for 90° are mixed. This can be seen in Figure 11 where data for 90° corresponding to the present cases of Figure 10 are plotted. The magnitudes are small exacerbating the scatter. Nevertheless, overall trends can still be discerned. For smaller values of $p_{\mu} d / p_j D$, there is a noise reduction (positive ordinates) but at higher values many of the cases exhibit a noise increase (negative ordinates).

It is noteworthy that most of the data from the literature pertain to lower values of $p_{\mu} d / p_j D$. In Reference 5, for example, noise reduction was shown to be practically uniform over all θ in two different facilities. With $p_{\mu} = 17.2$ bar and $d/D \approx 0.0075$ for either facility, $p_{\mu} d / p_j D$ turns out to be 0.075. At this abscissa value a reduction in the noise is also indicated in Figure 11 for all cases. Thus, it is possible that the noise increase at $\theta = 90^\circ$ may be characteristic of operation at high $p_{\mu} d / p_j D$.

At the highest value of $p_{\mu} d / p_j D \approx 0.16$ in Reference 4, the directivity data also showed a noise reduction practically over all θ (private communication). At corresponding location in Figure 11, the gaseous injection cases exhibit a noise increase. However, the present water injection data also exhibit a noise reduction (solid delta symbols). It was shown earlier in Reference 14 that with air injection often there is an increase in high frequency noise even though there was a reduction at lower frequencies and in OASPL. Comparison of spectra for water and air injection suggests a difference in the high-frequency ‘crossover’. This is shown by the spectra in Figures 12 and 13. The injection pressure was $p_{\mu} \approx 4500$ kPa for both air and water and the OASPL reduction at 25° was about the same. While the effect at low frequencies is similar there is a clear difference on the high frequency end. A crossover occurs under air injection but none with water. A similar observation is made from the 90° data in Figure 13. It appears that

the high frequency crossover is at least partly due to self noise from the μ jets. With gaseous flow the μ jets are in highly underexpanded supersonic condition and noisier. Comparatively, with water the flow is incompressible and there are no shocks or shock-associated noise. The self noise of the air μ jets is illustrated in Figure 14 illustrating elevated levels in the frequency range where the crossover takes place. Note, however, that simply a vector summation of the self noise with the baseline noise does not account for the total increase in the amplitudes. It appears that the flow interactions generate further high frequency noise which, intriguingly, is absent with the water injection.

3.3 Flowfields

A few aspects of the flowfield are now explored. Figure 15 shows pictures of the jet with water injection. In Figure 15(a), six 0.2 mm μ jets are injected at $p_\mu = 3200$ kPa. The individual μ jets can be seen near the nozzle that fills the core of the jet by about two diameters downstream. Subsequently, a jet of mist remains visible over a distance of tens of diameters. The trajectories of the μ jets in the vicinity of the nozzle were explored. Five of the ports were closed off and only one port was allowed to inject. The flow field was photographed with a camera-angle of 15° with respect to the nozzle exit plane; an example is shown in Figure 15(b). The trajectories of the outer edge of the μ jet were read off from the pixel counts in the digital pictures. Appropriate correction for the viewing angle was applied. The trajectories are shown in Figure 16 for different injection pressure (mPa), indicated in the legend. The lines through the data are ‘power function’ curve-fits. As expected, an increasing penetration with increasing p_μ is evident. Note that even at the highest p_μ ($= 10.6$ mPa) the μ jet is far from ‘piercing’ the primary jet. The jet centerline is at $y/d = 93$.

The penetration of the μ jet into the primary jet may be compared to available correlations for jet-in-a-crossflow. A set of data for $J = 20$ is shown in Figure 17. The (red) dotted curve represents text book correlation for subsonic air-in-air injection, $y/d = J^{0.33} (x/d)^{0.43}$ (Ref. 16). Note that a similar correlation was found to apply even with supersonic jets injected in supersonic crossflow (Ref. 17). Obviously, the water μ jet does not follow this correlation. The mixing rate of a liquid jet in a gaseous medium is slower, yielding much deeper penetration. The dashed curve for liquid-in-air injection follows the equation, $y/d = 1.55J^{0.53} \ln[1 + 1.66(x/d)]$, given in Reference 18. The present data are reasonably close to this curve.

The correlations noted above should also apply to the 0.1 mm port case. For $J = 20$, the value of $p_\mu d/p_j D$ with the 0.1 mm port is one-half of that with the 0.2 port (0.038 as opposed to 0.077). Conversely, for a constant $p_\mu d/p_j D$, the value of J is double with the smaller port. Using the correlation of Reference 18, the penetration at a fixed downstream distance of $x/D = 0.5$ can be calculated. For the 0.2 mm port with $J = 20$ the penetration is $y/D = 0.207$, whereas for the 0.1 mm port with $J = 40$ it would be $y/D = 0.169$. Since $p_\mu d/p_j D$ remains the same, this suggests that a given noise reduction may be achieved with different μ jet penetration depending on the port size. In other words, a larger noise reduction may not necessarily be due to a higher penetration of the μ jet.

Pitot probe surveys were conducted along the centerline of the jet. The data were converted to velocity assuming the static pressure to be the same as the ambient pressure. The results are shown in Figure 18. For the case without μ jets, a detailed profile was obtained under computer control. With the μ jets, only a few data points were acquired manually in order to conserve the bottle pressure. Two sets of data are shown with the pressures indicated in the legend. With μ jet injection a faster centerline decay of mean velocity is apparent; higher pressure causes faster jet decay.

A hot-film probe (TSI 1260-20) was used to measure the centerline variations of turbulence intensities. Note that in compressible flow a hot-wire responds to a combination of velocity and density fluctuations (with the high overheat ratio of 1.5 it is relatively insensitive to temperature fluctuation). First, variations in mean ρu are shown in Figure 19. These profiles correspond to the conditions of Figure 18 and exhibit distinct differences. The ‘potential core length’ for the baseline case turns out shorter with the hot-wire data. The Pitot probe velocity calculation assumes a constant ρ that actually

decreases with downstream distance relaxing to ambient level after several jet diameters. Moreover, the static pressure close to the nozzle usually is not the same as in the ambient—an assumption also made in the velocity calculation. On the other hand, the hot-film, which is calibrated against the plenum pressure by placing it at the nozzle exit, has its own problems. Besides sensor breakage in the high-speed flow, problems such as strain-gauging is often encountered that, in particular, affects the turbulence data. Nevertheless, the ρu data from the hot-wire are thought to be well represented whereas the ' U ' data from the Pitot probe clearly have errors primarily due to variation of ρ with x . In Figure 19, the jet decay with the μ jets at the lower pressure is found to be practically indistinguishable from the baseline case. However, at the higher pressure, a trend similar to that noted in Figure 18 is observed.

The root mean square (rms) fluctuation of ρu is shown in Figure 20. Relative to the baseline case, a distinct reduction in the turbulence is noted for both injection cases. A larger reduction in the peak level has taken place at the higher pressure. The turbulence data are commensurate with observations made by Arakari et al. (Ref. 6) using particle image velocimetry. As noted in that reference, the μ jets apparently disrupt the evolution of the large scale coherent structures causing a reduction in turbulence intensities that is accompanied by a reduction in jet noise.

3.4 A Few Implications of the Results

Recall that the parameter $p_\mu d/p_j D$ collapsed all data and the gaseous injection data also collapsed equally well with the parameter $\rho_\mu U_\mu d/\rho_j U_j D$. Also, by comparing Figures 6 and 9 it can be seen that the abscissa value for a given level of OASPL reduction with the gaseous cases is almost identical in the two figures, i.e., $p_\mu d/p_j D \approx \rho_\mu U_\mu d/\rho_j U_j D$. Let us examine this. Starting with compressible flow equations for pressure, temperature, and the equation of state, one can derive,

$$\rho_j U_j = p_j \sqrt{\frac{k}{R_1}} M_{ej} \left[1 + \frac{k-1}{2} M_{ej}^2 \right]^{-\frac{k+1}{2(k-1)}} \quad (2)$$

Here, ρ_j , U_j , and M_{ej} are density, velocity and Mach number at the exit of the primary jet, p_j is the total pressure driving the primary jet. (Note that the subscript ' e ' is dropped for the exit values of ρ and U for convenience). Using corresponding equation for the μ jet and assuming air-in-air injection one finds,

$$\frac{\rho_\mu U_\mu d}{\rho_j U_j D} = \frac{p_\mu d}{p_j D} \frac{M_{e\mu} \left[1 + \frac{k-1}{2} M_{e\mu}^2 \right]^{-\frac{k+1}{2(k-1)}}}{M_{ej} \left[1 + \frac{k-1}{2} M_{ej}^2 \right]^{-\frac{k+1}{2(k-1)}}} \quad (3)$$

For a subsonic primary jet, $M_{ej} = M_J$ by definition, and with injection from convergent ports, $M_{e\mu} = 1$. Therefore, for $M_J = 1$,

$$\frac{\rho_\mu U_\mu d}{\rho_j U_j D} \equiv \frac{p_\mu d}{p_j D} \quad (4)$$

At lower values of M_J , $\rho_\mu U_\mu d/\rho_j U_j D$ becomes slightly larger than $p_\mu d/p_j D$. For example, at $M_J = 0.95$ and 0.7 the ratio of the two parameters for air can be calculated from Equation (3) as 1.002 and 1.094, respectively. Thus, for the high subsonic jets considered here the two parameters are nearly equal. This is

why the abscissa values for the air injection cases are almost identical in Figures 6 and 9. For CO₂ injection, with $k = 1.3$ and $M_J = M_{e\mu} = 1$, one finds,

$$\frac{\rho_\mu U_\mu d}{\rho_j U_j D} = 0.9744 \frac{p_\mu d}{p_j D} \quad (5)$$

Thus, there is not much difference between the two parameters for CO₂ injection either. With water injection, on the other hand, the flow is incompressible and the relationship changes. With,

$$U_\mu = \sqrt{2p_\mu / \rho_\mu} \quad (6)$$

one can find,

$$C_1 \frac{\rho_\mu U_\mu^2 d}{\rho_j U_j^2 D} = \frac{p_\mu d}{p_j D} \quad (7)$$

Where,

$$C_1 = \frac{kM_J^2}{2} \left[1 + \frac{k-1}{2} M_J^2 \right]^{\frac{k}{k-1}} \quad (8)$$

For a given primary jet, C_1 is a constant. Thus, in contrast to Equations (3) to (5), the LHS of Equation (7) involves velocity-ratio-squared. Therefore, given that the data collapse with $p_\mu d / p_j D$, a deviation occurs with the water injection data when plotted as a function of $\rho_\mu U_\mu d / \rho_j U_j D$ (Fig. 6).

With regards to the dependence of the effect on J the following may be noted. For air-in-air injection, starting with Equation (3), and with $M_J = M_{e\mu} = 1$, one can show, $p_\mu d / p_j D = Jd/D$. With water injection, and for $M_J = 1$, it can be similarly shown that, $p_\mu d / p_j D = 0.37 Jd/D$. Thus, if the data of Figure 5 were plotted as a function of Jd/D the cases for air (as well as CO₂) would collapse while the water injection data would still remain separated. However, the separation would be only by a factor of about 0.37 and not by an order of magnitude as seen in Figure 6. The fact that the data would collapse with Jd/D once again implies the following. Depending on the port diameter, the same noise reduction would be achieved at different values of J . Since the trajectory of the μ jet is a unique function of J , one infers that the noise reduction may not be a direct function of the μ jet penetration.

Why is there a collapse of the data with $p_\mu d / p_j D$? Why is the noise reduction (ΔI), for a given primary jet, scale with $p_\mu d$? Unfortunately, the basic mechanism for turbulent mixing noise generation is not yet completely understood. Therefore, an understanding of the *noise reduction* with the μ jets remains even farther from being clear. In passing, one may note the following. For subsonic jets, experimentally it is known that OASPL (I) at a shallow angle scales as $M_J^{9.5}$ (e.g., Reference 19). Let us assume that the effective Mach number of the primary jet has dropped by ΔM under the influence of the μ jets. With $I = C_2 M_J^{9.5}$, where C_2 is a constant, one can show,

$$\Delta I = C_2 M_J^{9.5} \left[1 - \left(\frac{M_J - \Delta M}{M_J} \right)^{9.5} \right] \quad (9)$$

With $\Delta M \ll M_J$, this reduces to,

$$\Delta I = C_2 M_J^{8.5} \Delta M \quad (10)$$

Thus, if $p_\mu d$ were to reduce the jet Mach number by ΔM , the noise reduction by ΔI would be reconciled via Equation (10). If and why $p_\mu d$ might cause the jet Mach number to drop by ΔM remains unclear. The present as well as earlier measurements of Reference 6 indicate a clear reduction in jet turbulence under the influence of the μ jets. This perhaps is the most direct connection to the observed noise reduction. It is needless to reiterate that a full understanding of the noise reduction mechanism is considered beyond the scope of the present study.

Finally, let us examine some practical implications. Recall that smaller ports with higher pressure, involving less mass fraction and thrust, produce better noise reduction. First, with the observed scaling with $\rho_\mu U_\mu d / \rho_j U_j D$ for the gaseous injection, this is readily reconciled. Say, d/D is decreased and the pressure is increased such that the parameter $\rho_\mu U_\mu d / \rho_j U_j D$ remains a constant. Since d/D has been decreased, mass fraction ($= \rho_\mu U_\mu d^2 / \rho_j U_j D^2$) also has decreased. Thus, with a smaller mass fraction the same noise reduction is achieved since $\rho_\mu U_\mu d / \rho_j U_j D$ has been kept constant. Pushing this trend to extremes in applications, however, would have obvious limits. Perhaps, injector diameter less than 0.5 mm is not practical. Let us now consider the applicability of air injection to realistic engine conditions. Consider a 0.91 m (3-ft) diameter nozzle with hot flow at 593 °C (1100 °F). If one uses 18 ports with $d = 0.5$ mm, $\rho_\mu U_\mu d / \rho_j U_j D = 0.06$, (yielding 2.2 dB OASPL reduction per Equation (1) and recalling that it is for six injectors), would be achieved at about $p_\mu = 11.2$ mPa (1600 psig). With a compressed air reservoir of volume 0.0283 m³ (1 ft³), if one starts with 15.3 mPa (2200 psig), estimates show that the supply, that would have lasted 40 min in the model scale experiment (with eighteen 0.1 mm ports to yield the same amount of noise reduction), would be exhausted in about 35 sec. Obviously such a supply will not be adequate in practice and an alternative source will be required. It might be possible to have a small auxiliary compressor to provide high pressure at the small flow rates. Perhaps, the technique will work better in conjunction with other devices such as tabs/chevrons (Ref. 20). Periodic injection with small duty cycle, if effective, might cut down the flow-rate requirement drastically. As a noise reduction technique, the potential of μ jet injection would obviously require some further exploration and research.

Conclusions

The effect of μ jets injected from ports of different geometry on the radiated noise from a subsonic primary jet has been studied experimentally. Air, CO₂ and water were used as injection fluid while driving pressure up to 12.3 mPa was covered. A clear noise reduction is observed that improves with increasing μ jet pressure. It is found that smaller diameter ports with higher driving pressure, but involving less mass fraction and thrust, can produce better noise reduction. The results are examined in combination with air- as well as water-injection data from the literature. It is found that OASPL reduction at a shallow angle correlates with the ratio of μ jet to primary jet driving pressures normalized by the ratio of the corresponding diameters ($p_\mu d / p_j D$). When all data are plotted as a function of this parameter they collapse reasonably well. The OASPL reduction (in dB) in such a plot increases almost linearly with this parameter and a correlation equation is provided.

While $p_\mu d / p_j D$ collapses all data, the parameter $\rho_\mu U_\mu d / \rho_j U_j D$ is found to be equally effective for the gaseous cases. The water injection data, however, deviate from the gaseous cases when plotted as a function of the latter parameter. An analysis shows that for high subsonic primary jet and choked μ jets, the two parameters are nearly equal for the gaseous cases. With incompressible flow for the water μ jets, on the other hand, the two parameters are not equal. Thus, given that the data collapse with $p_\mu d / p_j D$, a deviation is noted for the water case when plotted as a function of $\rho_\mu U_\mu d / \rho_j U_j D$.

The scaling with $p_\mu d / p_j D$ is observed towards the jet's downstream direction and thus applies to turbulent mixing noise attenuation. At a measurement location perpendicular to the jet axis, the result is mixed and often an increase in the noise is noted. The collection of data suggests that the increase occurs

at large values of $p_{\mu}d/p_jD$ with the gaseous cases. Spectral analysis show that there is actually noise reduction at lower frequencies while a ‘crossover’ takes place at high frequencies, similar to observations made in previous studies with other devices such as tabs and chevrons. The increase in the high frequency amplitudes may offset the gain at low frequencies causing a net increase in OASPL. For water injection, on the other hand, no such high frequency crossover occurs and the attenuation in OASPL is observed throughout the parameter range. Spectra taken with air μ jets alone suggest that the high frequency crossover is at least partly due to self noise from the μ jets. The μ jets are in a highly underexpanded condition and apparently shock-associated noise adds to the total noise. For incompressible flow with water μ jets there is no shock-associated noise and, thus, no crossover at high frequencies.

Centerline velocity surveys made with a Pitot probe as well as a hot-film probe exhibit jet decay commensurate with the noise reduction at shallow angle. That is, larger noise reduction at higher $p_{\mu}d/p_jD$ is accompanied by faster jet decay. A physical basis why the noise reduction data correlate with the parameter $p_{\mu}d/p_jD$ remains unclear. A connection is seen from the flow data in that the μ jets substantially reduce jet turbulence. With increasing $p_{\mu}d/p_jD$ the centerline turbulence profiles exhibit decreasing peak amplitude that is accompanied by larger reduction in the mixing noise. Finally, possible application potential of the technique is discussed.

References

1. Zoppellari, E. and Juve, D., “Reduction of Hot Supersonic Jet Noise by Water Injection,” *AIAA Paper* 98-2204, 1998.
2. Krothapalli, A., Venkatakrisnan, L., Lourenco, L.M., Greska, B., and Elavarasan, R., “Turbulence and Noise Suppression of a High-Speed Jet by Water Injection,” *J. Fluid Mech.*, vol. 491, 2003.
3. Greska, B. and Krothapalli, A., “Jet Noise Reduction Using Aqueous Microjet Injection,” 10th AIAA/CEAS Aeroacoustics Conference, AIAA Paper 2004–2971, 2004.
4. Norum, T.D., “Reduction in Multi-component Jet Noise by Water Injection,” 10th AIAA/CEAS Aeroacoustics Conference, Manchester, U.K., *AIAA Paper* 2004–2976, 2004.
5. Greska, B., Krothapalli, A., Burnside, N., and Horne, W.C., “High-Speed Jet Noise Reduction Using Microjets on a Jet Engine,” 10th Aeroacoustics Conference, *AIAA Paper* 2004–2969, 2004.
6. Arakeri, V.H., Krothapalli, A., Siddavaram, V., Alkisar, M.B., and Lourenco, L.M., “On the Use of Microjets to Suppress Turbulence in a Mach 0.9 Axisymmetric Jet,” *J. Fluid Mech.*, vol. 490, 2003.
7. Alkisar, M.B., Krothapalli, A., and Butler, G.W., “The Effect of Streamwise Vortices on the Aeroacoustics of a Mach 0.9 Jet,” *J. Fluid Mech.*, vol. 578, 2007.
8. Callender, B., Gutmark, E. and Martens, S., “A Comprehensive Study of Fluidic Injection Technology for Jet Noise Reduction,” 13th AIAA/CEAS Aeroacoustics Conference, AIAA Paper 2007–3608, 2007.
9. Camussi, R., Guj, G., Tomassi, F., and Sisto, R., “Effect of Air Injection on the Far Field Pressure Radiated From a Jet at Subsonic Mach Numbers,” *Turbulent Jet Flows*, *Int. J. of Aeroacoustics*, vol. 7, no. 1, pp. 69–82, 2008.
10. Castelain, T., Sunyach, M., Juve, D. and Bera, J.-C., “Jet-Noise Reduction by Impinging Microjets: an Acoustic Investigation Testing Microjet Parameters,” *AIAA J.*, vol. 46, no. 5, May, 2008.
11. Kandula, M., “Prediction of Turbulent Jet Mixing Noise Reduction by Water Injection,” *AIAA J.*, 46(11), pp. 2714–2722, 2008.
12. Lilley, G.M., “Jet Noise Suppression Means,” 1961, U.S. Patent 2990905, (Ser. No. 733889, Claims Priority, application Great Britain May 13, 1957).
13. Henderson, B., “Over 50 Years of Fluidic Injection for Jet Noise Reduction,” *Int. J. of Aeroacoustics* (to appear), 2009.
14. Zaman, K.B.M.Q., 2007, “Subsonic Jet Noise Reduction by Microjets With Various Injection Port Geometry,” *AIAA Paper* 2007–3643, 13th AIAA/CEAS Aeroacoustics Conference, May 21–23, 2007, Rome, Italy.

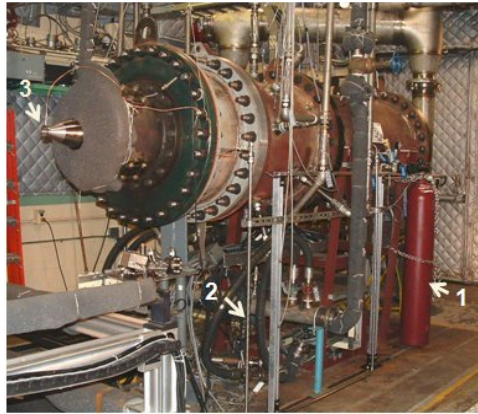
15. Zaman, K.B.M.Q. and Dahl, M., "Noise and Spreading of a Subsonic Coannular Jet—Comparison With Single Equivalent Jet," 43rd AIAA Aerospace Sciences Meeting, Reno, NV, Jan. 10–13, *AIAA Paper* 2005–0210, 2005.
16. Abramovich, G.N., "The Theory of Turbulent Jets," *The M.I.T. Press*, 1963.
17. Papamoschou, D. and Hubbard, D.G., 1993, "Visual Observations of Supersonic Transverse Jets," *Experiments in Fluids*, 14, pp. 468–476.
18. Tambe, S.B., Jeng, S.-M., Mongia, H. and Hsiao, G., 2005, "Liquid Jets in Subsonic Crossflow," 43rd AIAA Aerospace Sciences Meeting, Reno, NV, Jan. 10–13, *AIAA Paper* 2005–731.
19. Zaman, K.B.M.Q. and Yu, J.C., "Power Spectral Density of Subsonic Jet Noise," *J. Sound and Vib.*, 98, pp. 519–537, 1985.
20. Alkisar, M.B. and Butler, G.W., "Significant Improvements on Jet Noise Reduction by Chevron-Microjet Combination," *AIAA Paper* 2007–3598, 13th AIAA/CEAS Aeroacoustics Conference, May 21–23, 2007, Rome, Italy.

TABLE 1.—CALCULATED MASS FRACTION AND TOTAL THRUST OF μ JETS, RELATIVE TO PRIMARY JET, CORRESPONDING TO THE DATA OF FIGURE 3

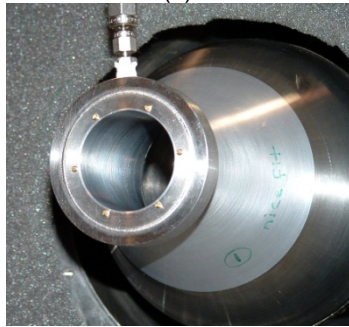
Number of ports	6	6
Port diameter, d (mm)	0.203	0.102
Pressure, p_u (kPa)	3410	6930
Momentum flux ratio, J	20	41
Mass fraction, m (percent)	0.34	0.17
Thrust fraction, t (percent)	0.60	0.30

TABLE 2.—OPERATING PARAMETERS FOR THE DATA FROM DIFFERENT SOURCES INCLUDED IN FIGURE 5

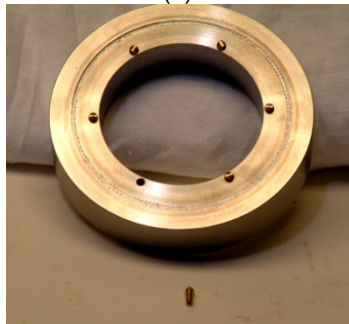
Work	M_j	D , mm	d , mm	n	θ
Present	0.95	37.6	0.203, 0.102	6	25
Reference 10 (CSJB)	0.90	50	0.7, 1, 1.3	18	30
Reference 6 (AKSL)	0.90	22.2	0.4	18	30
Reference 4 (TDN)	0.80	67.8	1.6	6	32



(a)

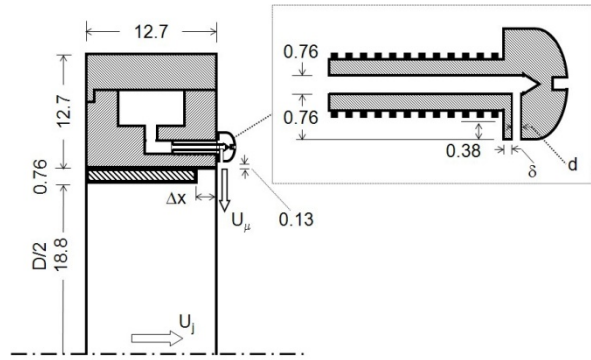


(b)

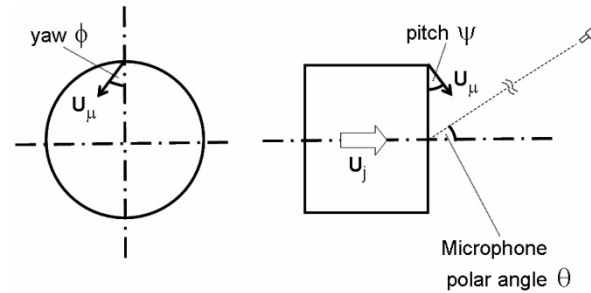


(c)

Figure 1.—Experimental setup. (a) Jet facility and auxiliary components: (1) compressed gas bottle, (2) U-tube used for water injection and (3) injector manifold. (b) Close-up picture of nozzle. (c) μ jet manifold.



(a)



(b)

Figure 2.—Schematic of nozzle and μ jet setup. (a) manifold details (0.76 mm is nozzle lip thickness, thus, μ jet travels 0.89 mm before impacting the jet), (b) definitions of μ jet yaw, pitch and microphone polar angle. Dimensions in mm.

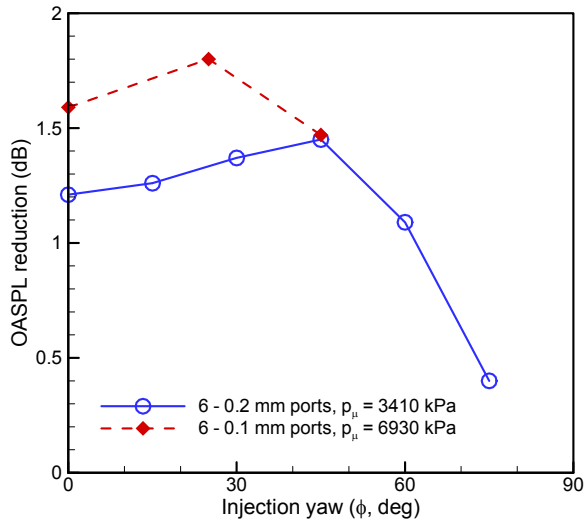


Figure 3.—OASPL reduction for varying yaw, for two port diameter cases from Reference 14; $\theta = 25^\circ$, $M_J = 0.95$.

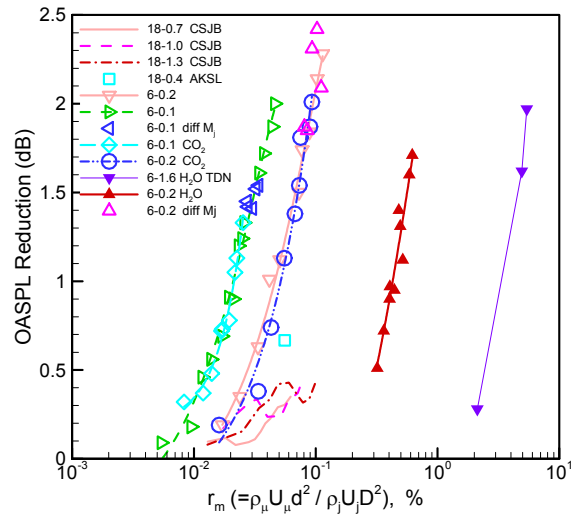


Figure 5.—Comparison of OASPL reduction versus mass fraction per μ jet, with data from Reference 6 (denoted AKSL), Reference 10 (denoted CSJB) and Reference 4 (denoted TDN).

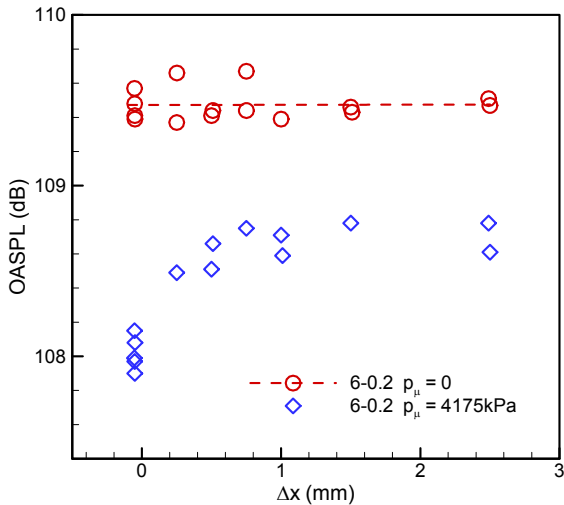


Figure 4.—OASPL at $\theta = 25^\circ$ for varying injection location, Δx , compared to no-injection case; six 0.2 mm ports, $M_J = 0.95$.

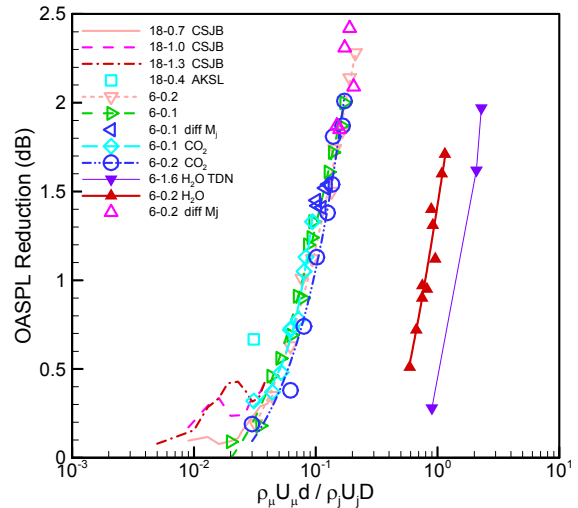


Figure 6.—OASPL reduction data of Figure 5 versus density-velocity-diameter-product ratio.

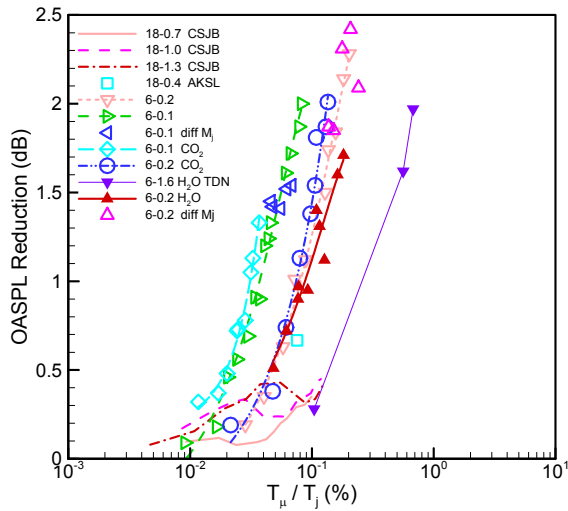


Figure 7.—OASPL reduction data of Figure 5 versus ratio of calculated total μ jet thrust to primary jet thrust.

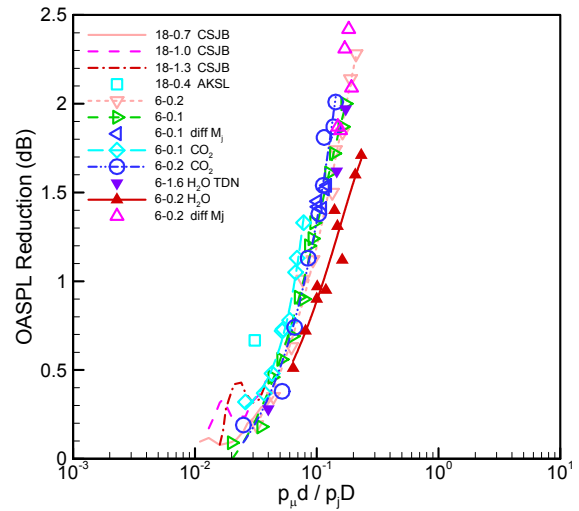


Figure 9.—OASPL reduction data of Figure 5 versus normalized ratio of driving pressures.

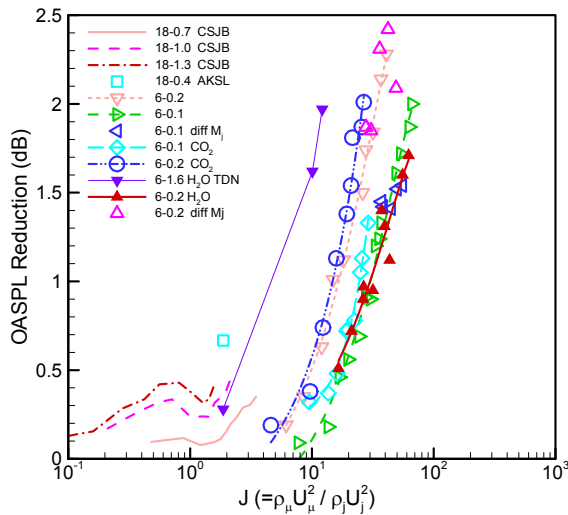


Figure 8.—OASPL reduction data of Figure 5 versus ratio of calculated momentum flux ratio.

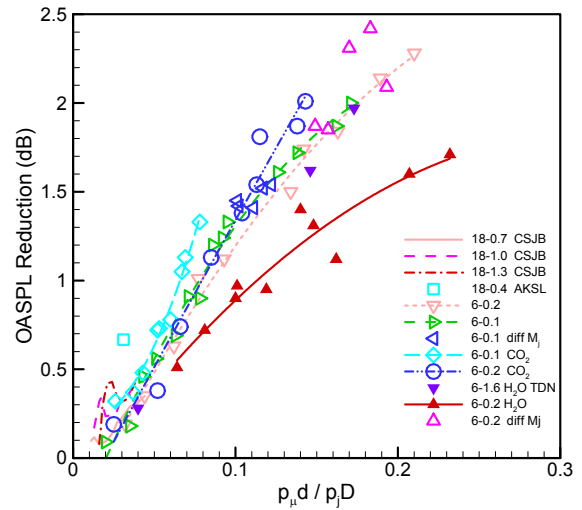


Figure 10.—Data of Figure 9 with linear expanded abscissa.

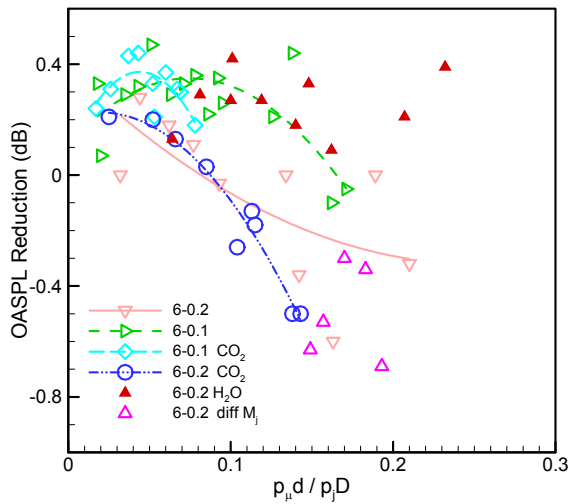


Figure 11.—OASPL reduction versus normalized ratio of driving pressures at $\theta = 90^\circ$, corresponding to a few cases of Figure 10.

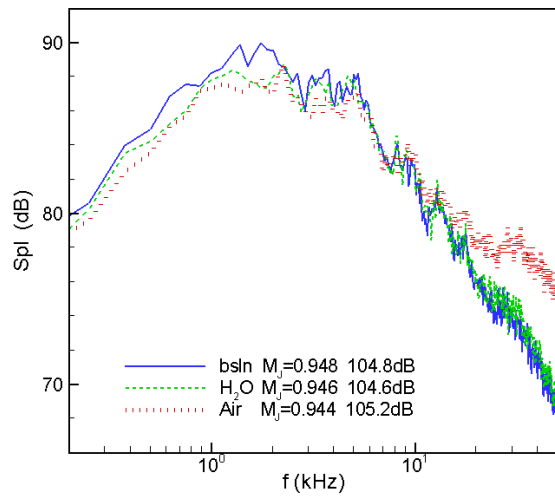


Figure 13.—Comparison of SPL spectra at $\theta = 90^\circ$ for air and water injection corresponding to the data of Figure 12.

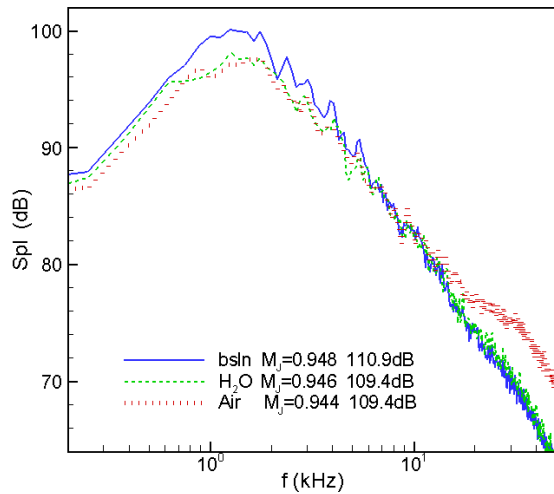


Figure 12.—Comparison of SPL spectra at $\theta = 25^\circ$ for air and water injection with the baseline (bsln) case; six 0.2 mm ports, $p_\mu \approx 4500$ kPa for both air and water.

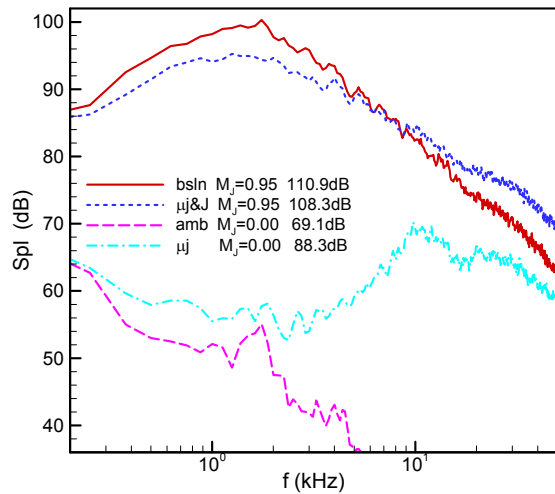


Figure 14.—SPL spectra at $\theta = 25^\circ$ with air injection at $p_\mu = 7830$ kPa (six 0.2 mm ports, denoted μ_j and J in legend) compared to baseline (bsln) case. The other two traces are for test chamber ambient condition (amb) and with only the μ_j jets running at 6840 kPa (μ_j).

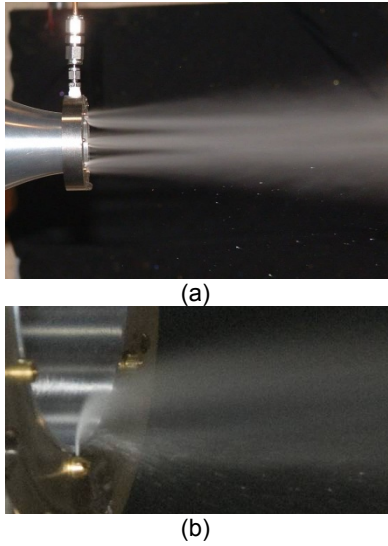


Figure 15.—Picture of jet at $M_J = 0.95$ with water injection; (a) injection from six 0.2 mm ports at $p_{in} = 3200$ kPa, (b) one 0.2 mm port at $p_{in} = 5600$ kPa.

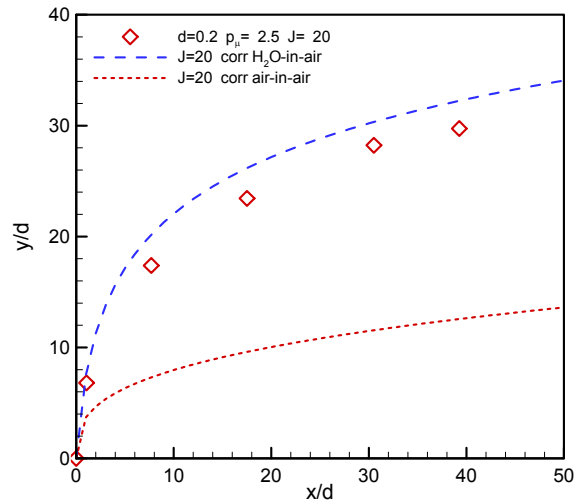


Figure 17.—Trajectory of water μ jet at $J = 20$ for a 0.2 mm port; $M_J = 0.95$. Correlation for H_2O -in-air is from Reference 18 and that for air-in-air is from Reference 16.

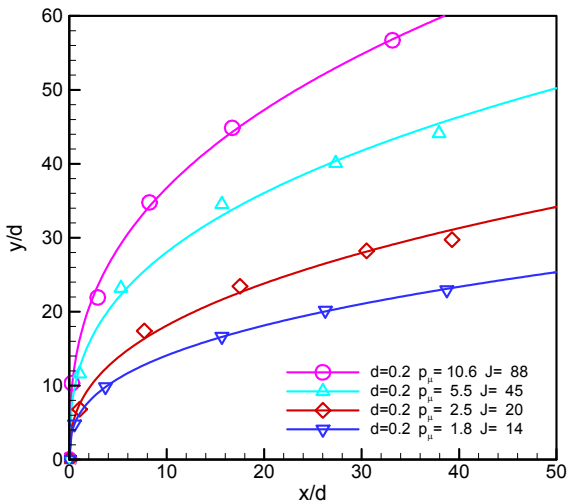


Figure 16.—Trajectories of water μ jet from a 0.2 mm port into the $M_J = 0.95$ jet for various injection pressures (mPa).

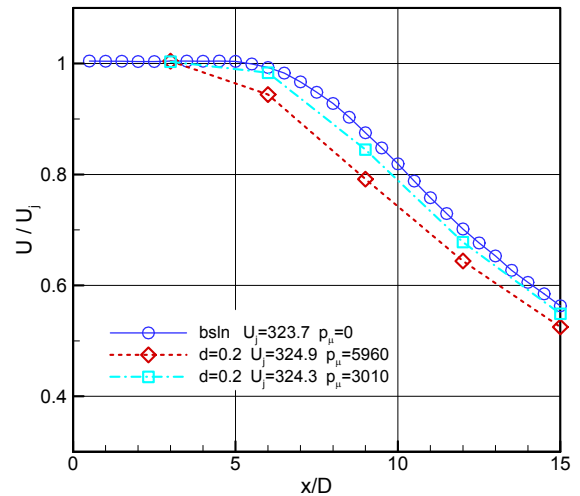


Figure 18.—Centerline velocity as estimated from Pitot probe measurement for indicated injection pressures; six 0.2 mm (air) μ jets, $M_J = 0.95$.

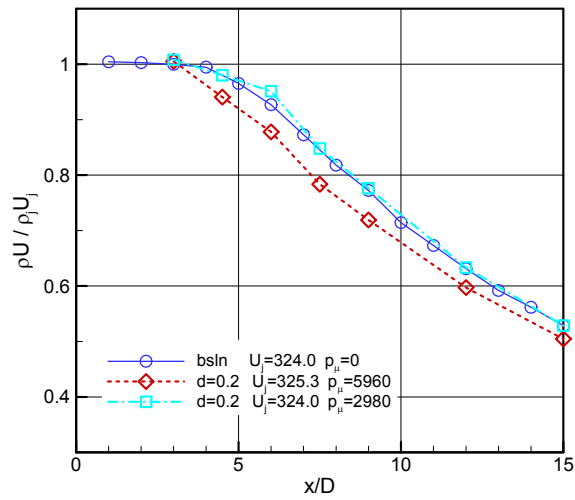


Figure 19.—Centerline variations of mean hot-wire output for indicated injection pressures corresponding to the cases of Figure 18.

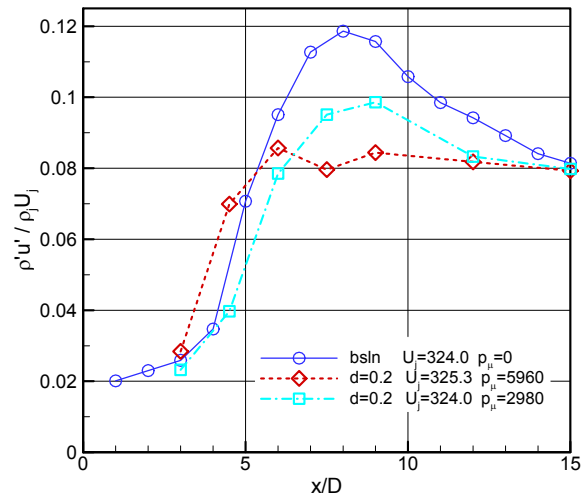


Figure 20.—Centerline variations of the rms of hot-wire output corresponding to the cases of Figure 19.

REPORT DOCUMENTATION PAGE			Form Approved OMB No. 0704-0188		
<p>The public reporting burden for this collection of information is estimated to average 1 hour per response, including the time for reviewing instructions, searching existing data sources, gathering and maintaining the data needed, and completing and reviewing the collection of information. Send comments regarding this burden estimate or any other aspect of this collection of information, including suggestions for reducing this burden, to Department of Defense, Washington Headquarters Services, Directorate for Information Operations and Reports (0704-0188), 1215 Jefferson Davis Highway, Suite 1204, Arlington, VA 22202-4302. Respondents should be aware that notwithstanding any other provision of law, no person shall be subject to any penalty for failing to comply with a collection of information if it does not display a currently valid OMB control number.</p> <p>PLEASE DO NOT RETURN YOUR FORM TO THE ABOVE ADDRESS.</p>					
1. REPORT DATE (DD-MM-YYYY) 01-02-2010		2. REPORT TYPE Technical Memorandum		3. DATES COVERED (From - To)	
4. TITLE AND SUBTITLE Jet Noise Reduction by Microjets--A Parametric Study			5a. CONTRACT NUMBER		
			5b. GRANT NUMBER		
			5c. PROGRAM ELEMENT NUMBER		
6. AUTHOR(S) Zaman, K.B.M.Q.			5d. PROJECT NUMBER		
			5e. TASK NUMBER		
			5f. WORK UNIT NUMBER WBS 984754.02.07.03.17.04		
7. PERFORMING ORGANIZATION NAME(S) AND ADDRESS(ES) National Aeronautics and Space Administration John H. Glenn Research Center at Lewis Field Cleveland, Ohio 44135-3191			8. PERFORMING ORGANIZATION REPORT NUMBER E-17112		
9. SPONSORING/MONITORING AGENCY NAME(S) AND ADDRESS(ES) National Aeronautics and Space Administration Washington, DC 20546-0001			10. SPONSORING/MONITOR'S ACRONYM(S) NASA		
			11. SPONSORING/MONITORING REPORT NUMBER NASA/TM-2010-215846		
12. DISTRIBUTION/AVAILABILITY STATEMENT Unclassified-Unlimited Subject Categories: 71 and 34 Available electronically at http://gltrs.grc.nasa.gov This publication is available from the NASA Center for AeroSpace Information, 443-757-5802					
13. SUPPLEMENTARY NOTES					
14. ABSTRACT The effect of injecting tiny secondary jets ('μjets') on the radiated noise from a subsonic primary jet is studied experimentally. The μjets are injected on to the primary jet near the nozzle exit with variable port geometry, working fluid and driving pressure. A clear noise reduction is observed that improves with increasing μjet pressure. It is found that smaller diameter ports with higher driving pressure, but involving less thrust and mass fraction, can produce better noise reduction. A collection of data from the present as well as past experiments is examined in an attempt to correlate the noise reduction with the operating parameters. The results indicate that turbulent mixing noise reduction, as monitored by OASPL at a shallow angle, correlates with the ratio of μjet to primary jet driving pressures normalized by the ratio of corresponding diameters ($p_{\mu}d/p_jD$). With gaseous injection, the spectral amplitudes decrease at lower frequencies while an increase is noted at higher frequencies. It is apparent that this amplitude 'crossover' is at least partly due to shock-associated noise from the underexpanded μjets themselves. Such crossover is not seen with water injection since the flow in that case is incompressible and there is no shock-associated noise. Centerline velocity data show that larger noise reduction is accompanied by faster jet decay as well as significant reduction in turbulence intensities. While a physical understanding of the dependence of noise reduction on $p_{\mu}d/p_jD$ remains unclear, given this correlation, an analysis explains the observed dependence of the effect on various other parameters.					
15. SUBJECT TERMS Jets; Noise; Shocks; Turbulence					
16. SECURITY CLASSIFICATION OF:			17. LIMITATION OF ABSTRACT UU	18. NUMBER OF PAGES 25	19a. NAME OF RESPONSIBLE PERSON STI Help Desk (email:help@sti.nasa.gov)
a. REPORT U	b. ABSTRACT U	c. THIS PAGE U			19b. TELEPHONE NUMBER (include area code) 443-757-5802

